AGU100 ADVANCING EARTH AND SPACE SCIENCE

Water Resources Research

RESEARCH ARTICLE
10.1029/2017WR022356

# Groundwater Subsidy From Headwaters to Their Parent Water Watershed: A Combined Field-Modeling Approach

A. A. Ameli[1], C. Gabrielli[1], U. Morgenstern[2], and J. J. McDonnell[1,3,4]

[1]Global Institute for Water Security, University of Saskatchewan, Saskatoon, Saskatchewan, Canada, [2]GNS Science, Avalon, Lower Hutt, New Zealand, [3]School of Resources and Environmental Engineering, Ludong University, Yantai, China, [4]School of Geography, Earth & Environmental Sciences, University of Birmingham, Birmingham, UK

**Key Points:**
- More than 50% of recharge within the Maimai headwaters discharges into their parent watershed
- This groundwater subsidy from headwaters to parent watershed can be hundreds of years old
- Recharge rate and watershed slope appear to control the age and magnitude of groundwater subsidy

**Supporting Information:**
- Supporting Information S1

**Correspondence to:**
A. A. Ameli,
ali.ameli@usask.ca

**Citation:**
Ameli, A. A., Gabrielli, C., Morgenstern, U., & McDonnell, J. J. (2018). Groundwater subsidy from headwaters to their parent water watershed: A combined field-modeling approach. *Water Resources Research*, *54*. https://doi.org/10.1029/2017WR022356

Received 4 DEC 2017
Accepted 25 JUN 2018
Accepted article online 2 JUL 2018



**Abstract** Headwater groundwater subsidy, defined here as out-of-catchment groundwater flow contribution from a headwater catchment to its larger parent watershed (i.e., higher-order stream), can influence the water quality and quantity of regional water resources. But the integrated flow and transport modeling approaches currently being implemented to quantify this subsidy are limited by an absence of critical field observations, such as water table dynamics and groundwater age that are required to test such models. Here we couple tracer (and hydrometric) observations from the well-studied 4.5-ha M8 headwater catchment in the Maimai experimental watershed with a new semianalytical free-surface integrated flow and transport model. Our main research goals are to quantify the magnitude, age, and flow paths of the headwaters groundwater subsidies at the Maimai experimental watershed. Additionally, we explore through virtual experiments the effects of watershed slope, watershed active thickness, and recharge rate on the age, flow path, and magnitude of out-of-catchment headwater groundwater subsidies versus within-catchment (or local) groundwater flow contributions. Our results show that more than 50% of groundwater recharged in the Maimai headwaters subsidizes their parent watershed. The relative proportion of headwaters groundwater subsidies is inversely proportional to recharge rate and/or directly proportional to slope angle. Our results also show that the age of the headwater groundwater subsidies is more than 500 years, almost 9 times older than the age of within-catchment groundwater flow contributions. These findings highlight the need to consider headwaters groundwater subsidies in groundwater management area considerations.

## 1. Introduction

Significant strides have recently been made in modeling the links between topography, geology, climate, and groundwater across multiple scales (e.g., Condon & Maxwell, 2015; Gleeson et al., 2016; Maxwell et al., 2015; Zech et al., 2016). Many of these works build on decades of research with integrated flow and transport models that have helped reveal the linkages between watershed-scale processes and regional and local scale groundwater systems (as outlined in M. P. Anderson et al., 2015). Since the early benchmark works of Toth (1963) and Freeze and Witherspoon (1967), useful simulations of steady state local and regional groundwater flow and transport have been conducted using analytical and numerical modeling approaches (Ameli et al., 2013; Cardenas & Jiang, 2010; Fiori & Russo, 2008; Janković et al., 2003; Marklund & Wörman, 2011).

One key issue in recent groundwater research is the quantification of *headwater groundwater subsidy*, defined as out-of-catchment groundwater flow contribution from a headwater catchment to higher-order lower-elevation stream (Hwang et al., 2012). This subsidy has been shown anecdotally to impact (1) water quality in the higher-order streams (Ameli et al., 2017; Jasechko et al., 2016; Winter et al., 2003), (2) the fate and biogeochemical alteration of nonpoint source agricultural pollution (Pinay et al., 2015; Thomas et al., 2016; Van Meter et al., 2018; Weyer et al., 2014), (3) the water replenishment in economically important aquifers within arid and semiarid mountainous regions (Manning & Solomon, 2005; Wilson & Guan, 2004), (4) the generation and migration of petroleum and mineral deposits (Person et al., 1996), and (5) the ecological functioning (e.g., transpiration) of the watershed (Golden et al., 2017; Hayashi & Rosenberry, 2002; Maxwell & Condon, 2016). For example, Genereux et al. (2002) showed, in a coastal plain watershed in Costa Rica, that while 49% of water in the watershed's regional water body was derived from regional groundwater flow, 99% of the water body's chloride was derived from distant upland headwater groundwater sources.

But while recent studies have shown the importance of headwaters groundwater subsidies to their parent watersheds, the timing, flow paths, and age of the linkages between groundwater in steep headwaters and their parent watersheds are poorly understood but critically required for predicting the watershed biogeochemical processes (e.g., Pinay et al., 2015) and sensitivity to environmental changes (e.g., Carey et al., 2010), as well as for designing reliable water quality policy (Van Meter et al., 2018) and understanding the synchronicity between water quality and water quantity responses (Hrachowitz et al., 2016; McDonnell & Beven, 2014).

Quantifying the magnitude, age, and flow paths of headwaters groundwater subsidies to their larger parent watershed is a major research challenge. But how can we do this? While pure modeling approaches provided useful insights into the general behavior of regional-scale groundwater flow and the controls on the magnitude of regional-scale groundwater flow (e.g., Gleeson & Manning, 2008), they do not reveal the realities of storage and release within the headwaters nor the measured flow paths and ages that are needed to sufficiently define groundwater contributions from headwaters to higher-order streams. At the same time, purely experimental approaches have shown that headwaters groundwater contributions to higher-order lower-elevation streams are nontrivial (e.g., Gardner et al., 2011; Harrington et al., 2014; Smerdon et al., 2012), but they are unable to account for the full suite of flow paths and transport connections given instrumentation restrictions. In addition, practical restrictions such as spatiotemporal variability of tracer measurements and the short time to equilibrium of some tracers (e.g., $^{222}$Rn; Harrington et al., 2014; McCallum et al., 2015; Smerdon et al., 2012) often limit the applicability of purely tracer-based experimental approaches to characterize headwaters groundwater subsidies.

Here we take a hybrid approach that combines a dense field-based data set from a bedrock drilling campaign at the Maimai watershed in New Zealand (for a review, see McGlynn et al., 2002) with the new physically based semianalytical integrated flow and transport model of Ameli and Craig (2014). We use this hybrid approach to validate the findings of previous theoretical studies on the magnitude of regional groundwater flow and to calculate the age and flow paths of groundwater subsidies from the Maimai headwaters to the larger Maimai watershed.

Our model has a free-surface and meshless design that allows for efficient simulation of water table location as well as water particle tracking to generate local and regional groundwater flow paths and ages. We start by testing the model against observed groundwater flow and transport processes in the M8 headwater catchment within the Maimai watershed. To do this, we use observed water table measurements in combination with tracer-based estimation of groundwater ages from newly drilled bedrock wells (Gabrielli, 2017). We then performed a series of virtual experiments (following Weiler & McDonnell, 2004) to explore the factors controlling the age and magnitude of headwaters groundwater subsidies to their larger parent watershed. Our main questions are the following:

1. Does our semianalytical model capture observed water table location and tracer-based estimations of groundwater ages (and transit times)?
2. What are the magnitude, age, and flow paths of the groundwater subsidies from the Maimai headwater catchments (including M8 catchment) to the larger Maimai watershed?
3. How are the patterns, fluxes, and age of headwaters groundwater subsidies to their larger parent watershed influenced by the annual groundwater recharge rate, watershed slope, and watershed active layer thickness?

## 2. Materials and Methods

### 2.1. Study Site

The 280-ha Maimai experimental watershed is located on the northwest coast of the South Island, New Zealand (Figure 1; 42°05′S 171°47′E). The Maimai watershed is composed of approximately 28 small headwater catchments ranging in size from 1 to 17 ha. Most catchments are aligned orthogonal to the main valley drainage system (called Powerline Creek). Elevation ranges from 225 to 402 m above sea level. The landscape is highly dissected and dominated by three main geomorphic landscape units: highly convergent and divergent hillslopes, steep ephemeral hollows, and relatively gently sloping riparian zones (Weiler et al., 2003). Hillslopes are short (~50–100 m) and steep (range: 15° to 65°, average: 38°). Annual rainfall is 2,600 mm occurring over 186 days/year on average (Neary et al., 1978). Annual runoff and base flow at the watershed outlet are estimated as 1,660 and 624 mm, respectively (McGlynn et al., 2004; Pearce et al., 1986).

10.1029/2017WR022356

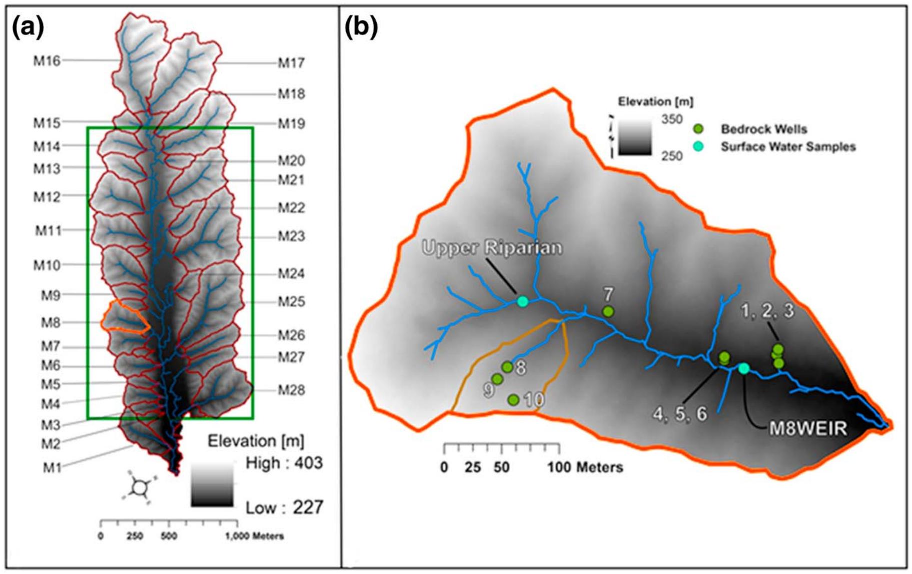


**Figure 1.** The layout of the Maimai watershed. (a) The entire watershed with each headwater catchment labeled. The green rectangle depicts the computational domain, and the orange boundary shows the position of the M8 catchment within the larger Maimai watershed. The main valley drainage network of the Maimai watershed is known as Powerline Creek. (b) the M8 catchment and the location of measurement stations. The locations of the sampled bedrock wells are labeled as 1–10. Surface water samples were collected during a base flow period from the main M8 catchment weir (M8WEIR) and from surface flow at the location marked as Upper Riparian.

The soil and bedrock geology are relatively uniform (McGlynn et al., 2004). Soils are thin, averaging 0.6 m and ranging from 0.1 to 1.8 m, and are highly transmissive. The early Pleistocene conglomerate forms the bedrock, known as the Old Man Gravel formation. This formation is composed primarily of sandstone clasts embedded in a consolidated sandy-clay matrix (Bowen, 1967). Bowen (1967) suggests that the upper part of this formation is characteristically weathered to a rusty yellow-brown with a thickness of less than 120 m at Jones Creek and Donnelly Creek, 110 km north and 145 km south of the Maimai watershed, respectively. In Donnelly Creek, the total thickness of the bedrock formation is estimated to be on the order of 250 m (Bowen, 1967). Bedrock porosity—determined from lab based water displacement tests (Gabrielli, 2017)—is on average 0.205. For this measurement, three 0.05-$m^3$ bedrock samples were extracted from the bedrock surface within the M8 headwater catchment using a concrete cutting saw (measured porosities were 0.205, 0.197, and 0.210).

## 2.2. Field Analysis

Field analysis for this study focused primarily on the 4.5 ha M8 catchment within the larger Maimai experimental watershed (Figure 1b). M8 has been studied intensively for more than 40 years, providing considerable insights on subsurface runoff generation (Mosley, 1979; Pearce et al., 1986), the effusion of old water (McDonnell, 1990), and the transient spatial and temporal source components of stormflow (McGlynn et al., 2004). In 2014, 40 wells were drilled and completed within the M8 bedrock. These wells were used for hydraulic conductivity and ground water table measurements, as well as for tritium-based age estimates on groundwater samples (section 2.3). We focused on 10 deep observation wells drilled from 3 to 9.5 m below the ground surface and located in riparian, hollow, and hillslope positions (Figure 1b). To isolate the effect of groundwater flow from shallower subsurface flow, we focused on observations made on 24 February 2015 of water table and groundwater age during a time of extremely low flow when the catchment was in deep base flow conditions. The age of water along the M8 stream network was also estimated based on tritium observations on the same day at two surface locations (M8 Weir and Upper Riparian in Figure 1b).

In addition, we used 13 years (1975–1987) of discharge records from the M8 Weir (supporting information Figure S1a) to estimate base flow (Figure S1b). To do this, we employed the Web-Based Hydrograph Analysis Tool's base flow separation package (Lim et al., 2005). Low base flow (10th

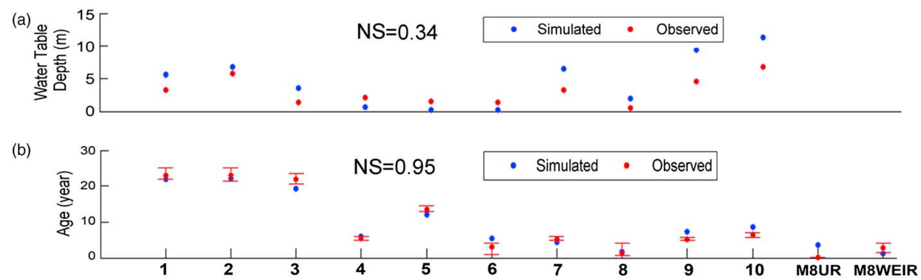


**Figure 2.** Simulated and observed (or estimated) groundwater table depths, groundwater ages and transit times at measurement locations. (a) Performance of the calibrated model in emulating the observed groundwater table depths at 10 measurement locations in the bedrock. (b) Performance of the calibrated model in emulating the tracer-based estimates of groundwater ages and stream water transit times at 12 measurement locations in the bedrock and stream. The bars show the uncertainty range for estimated ages and transit times. NS = Nash-Sutcliffe; UR = Upper Riparian.

percentile), average base flow, and high base flow (90th percentile) over 13 years equaled 4, 365, and 730 mm/year, respectively. Median base flow was also estimated as 165 mm/year. The coefficient of variation of estimated base flow was 5% between 1975 and 1987.

### 2.3. Tracer-Based Groundwater Age (and Transit Time) Estimates

We estimated tritium-based groundwater ages and surface water transit times using the convolution approach (Małoszewski & Zuber, 1982) with an exponential piston flow model (EPM). To select EPM exponential flow volume parameter, we performed a sensitivity analysis for the Maimai groundwater age and transit time estimates for a sensible range of EPM exponential flow volume parameter (40–90%). This analysis showed that only for very old waters the ages were sensitive to the choice of the exponential flow volume parameter. To enable comparison between the water samples, we consistently used an EPM model with 70% exponential flow volume parameter for all samples. Note that the assessment of over a hundred long-term time series data from groundwater discharges in New Zealand, covering the time of the tritium-pulse, indicated that the EPM with 70% exponential flow volume parameter provides a realistic age distribution for hydrogeologic settings similar to the Maimai watershed (Morgenstern & Daughney, 2012).

Tritium measurements in rainfall were available from monthly rain samples since 1960, and tritium concentrations in groundwater and stream water were measured in samples collected from groundwater wells and stream in the Maimai catchment between February 2015 and February 2016. Tritium analysis was done using liquid scintillation counting in Quantulus ultralow-level counters following vacuum distillation and electrolytic enhancement (Morgenstern & Taylor, 2009). Low uncertainty of tritium measurements was achieved by tritium enhancement by a factor of 95 which yields a detection limit of 0.02 tritium units. Although tritium age interpretations are still ambiguous in the Northern Hemisphere and require tritium time series or multitracer data, in the Southern Hemisphere, the amount of tritium in the atmosphere has already decayed to insignificant levels so that it no longer causes ambiguity in the age interpretation (Morgenstern & Daughney, 2012). The calculated range of uncertainty for age estimation in this study is comparable to similar studies in the other sites (Cartwright et al., 2018, and references therein). Figure 2 shows the estimates of groundwater ages (and transit times) and their uncertainty at different locations.

### 2.4. Modeling Groundwater-Surface Water Interaction and Groundwater Age

#### 2.4.1. Semianalytical Groundwater-Surface Water Interaction Model

We used the semianalytical 3-D groundwater-surface water interaction method described by Ameli and Craig (2014) to simulate local and regional scale groundwater flow at the Maimai watershed and its headwater catchments. This physically based, meshless method exactly satisfies the governing equation of the steady state saturated flow in each layer of an unconfined aquifer. This method uses a free-surface boundary condition (Bear, 1972; Bresciani et al., 2016) to calculate the location of the water table. This condition is iteratively imposed using a recharge-water table depth relation scheme presented in Ameli and Craig (2014) that creates a spatially variable recharge rate and enables delineation of discharge areas where the water table reaches the land surface. At each iteration, recharge rate is constant in most parts of the recharge areas (with a rate equal to maximum recharge rate) but smoothly decreases in the vicinity of discharge areas wherein the water table approaches the land surface. The iterations continue until pressure head along the a priori unknown water table location converges to zero (average pressure head in the entire watershed becomes $<0.001$ m).

The modeled computational domain was assumed rectangular with a length of $L_x$ = 1,150 m and width of $L_y$ = 2,200 m (Figure 1a). The computational domain in the vertical direction consisted of a two-layer system represented by a more permeable bedrock formation with a thickness of 100 m overlaying a potentially less permeable bedrock formation. The top boundary was the digital elevation model-based ground surface. The no-flow bottom boundary of the computational domain was assumed to be at $Z = 0$ in the reference example solved in this paper. This treatment leads to a varying aquifer thickness from 225 to 402 m with an average thickness of 302 m for the computational domain. The model structure and thickness is consistent with available information on the Maimai watershed bedrock geology as explained in section 2.1. In addition, no-flow boundary conditions were imposed along the four sides of the rectangular computational domain.

The mathematical formulation and solution parameters of this model as well as the implementation of the boundary conditions, including free-surface condition to locate the water table, are explained in Text S1. The model provides continuous maps of subsurface mean pore water velocities in *x*, *y*, and *z* directions (equation (A.4) in Text S2), and this information is used to track water particles and model groundwater age and transit time.

#### 2.4.2. Random Walk Particle-Tracking Method to Model Groundwater Age and Transit Time

Water particle release points in the forward tracking approach used here were placed uniformly and spaced 10 m along the land surface. In the *unsaturated zone*, particles were assumed to move vertically with a velocity of 1 m/year (see Text S2 for more details). This velocity is consistent with bedrock characteristics observed at the ridge line of the M8 catchment where Gabrielli (2017) used tritium-based groundwater age dating and bedrock porosity measurements to determine recharge rates. In the *saturated zone*, continuous mapping of steady state saturated velocity in *x*, *y*, and *z* directions ($V^x(x, y, z)$, $V^y(x, y, z)$, and $V^z(x, y, z)$, respectively; equation (A.4)) was used to track water particles using the following particle-tracking approach:

$$x_p(t) = x_p(t-\Delta t) + V^x\Big(x_p(t-\Delta t), y_p(t-\Delta t), z_p(t-\Delta t)\Big)*\Delta t, \tag{1a}$$

$$y_p(t) = y_p(t-\Delta t) + V^y\Big(x_p(t-\Delta t), y_p(t-\Delta t), z_p(t-\Delta t)\Big)*\Delta t, \tag{1b}$$

$$z_p(t) = z_p(t-\Delta t) + V^z\Big(x_p(t-\Delta t), y_p(t-\Delta t), z_p(t-\Delta t)\Big)*\Delta t, \tag{1c}$$

where $x_p(t)$, $y_p(t)$, and $z_p(t)$ are the positions of the particle *p* at time *t*, and $x_p(t-\Delta)$, $y_p(t-\Delta)$, and $z_p(t-\Delta)$ are the positions of the particle *p* at time $t-\Delta$. In the particle-tracking algorithm, a small time step ($\Delta = 0.001$ day) was assumed to ensure the precise calculation of the particle's location and movement.

Along the generated pathlines, equations (1a)–(1c) determine groundwater flow length and transit time from recharge zones to discharge interfaces and can also determine these at any point of interest within the subsurface domain. Here we define water transit time ($\tau$) through the system following the nomenclature of McDonnell et al. (2010) as $\tau = t_{out} - t_{in}$ where $\tau$ is the elapsed time from the input of a water parcel through a system input boundary at time $t_{in}$ to the output of that water parcel through a system output boundary (e.g., stream) at time $t_{out}$. We also follow the McDonnell et al.'s (2010) definition of age of a water parcel sampled at any location W (*x*, *y*, and *z*) within the catchment system. The age of a water parcel at location W (*x*, *y*, and *z*) is then defined as $\tau_W = t_W - t_{in}$, where $\tau_W$ is the elapsed time from the input of water parcel through the catchment to the arrival time ($t_W$) of that water parcel at location W. As noted in McDonnell et al. (2010, p. 1746) "the transit time is thus the age at the exit of the system. Similarly, the age of water sampled at an observation well within a catchment represents the transit time for water through the catchment area to that well."

For each example solved here, we calculated the median transit time ($M_{ed}$TT) and median flow length ($M_{ed}$FL) corresponding to all pathlines between recharge and discharge zones (e.g., stream). In this paper, we used $M_{ed}$TT, rather than the widely used "mean transit time" (cf. McGuire & McDonnell, 2006), as the median of simulated transit times more realistically represents age-related observations in the shallow subsurface or stream network, given the extremes when looking in terms of *age* (i.e., very old water particles stored in deep groundwater reservoirs), because a mean would be biased to these extremes. Berghuijs and Kirchner (2017) theoretically proved that the age of deep groundwater can be an order of magnitude older than the age of the water that we measure in the stream network. In addition, for each example solved in this paper, we calculated $M_{ed}TT$ and discharge rate at 100 points located longitudinally along the main valley drainage network of the Maimai watershed (Powerline Creek). For each example, the simulated $M_{ed}TTs$ and discharge rates were then used to calculate the coefficient of variation of the transit times and discharge rates along the length of Powerline Creek.

The modeling approach uses a steady state assumption and homogenous and laterally constant material property within each layer of bedrock formation. The validity of the employed assumptions are supported by existing observations in the Maimai watershed. Minimal variation in long-term base flow (5% coefficient of variation between 1975 and 1987) also supports the validity of the steady state assumption for groundwater flow and discharge behavior, within a bedrock with an unusually homogenous geology (Pope et al., 2000), and uniform lateral pattern of saturated hydraulic conductivity (Bowen, 1967; McGlynn et al., 2004).

### 2.5. Model Testing

We calibrated our model to calculate (1) the saturated hydraulic conductivities of the top layer ($K_t$) and the bottom layer ($K_b$) of the bedrock formation and (2) the maximum recharge rate ($R$), using measured field data from the M8 catchment. Note that the saturated hydraulic conductivities are assumed to be constant in each bedrock layer. In addition, the maximum recharge rate refers to the recharge rate applied along the most parts of the recharge areas where the water table is well below the land surface. The maximum recharge rate decreases in the vicinity of discharge areas where the water table approaches the land surface using the recharge-water table scheme presented in Ameli and Craig (2014).

To constrain the range of parameters in a manual calibration, we used available measurements and estimations of saturated hydraulic conductivities and recharge rates. Saturated hydraulic conductivity of the upper portion of bedrock formation was measured at 40 well locations using falling head slug tests. Values ranged from $6.99 \times 10^{-9}$ to $4.01 \times 10^{-5}$ m/s and averaged $5 \times 10^{-7}$ m/s. A plot-scale hillslope sprinkler experiment was also conducted on an open bedrock surface, as outlined in Gabrielli (2017), which identified a mean percolation rate of $5.69 \times 10^{-8}$ m/s. We therefore used a range from $1 \times 10^{-6}$ to $1 \times 10^{-9}$ m/s for the calibration of $K_t$. The range of saturated hydraulic conductivities for the calibration of lower portion of bedrock formation ($K_b$) were assumed from $1 \times 10^{-7}$ to $1 \times 10^{-10}$ m/s. Using available observations, we roughly estimated bedrock groundwater recharge rates of 167 mm/year through the application of a simple Darcy-based flux approximation and 216 mm/year using a tritium-based groundwater transit time approach (Text S2). We therefore used a range from 167 to 216 mm/year for the calibration of maximum recharge rate ($R$) within our semianalytical model.

The performance of the calibrated model was assessed for its ability to (1) simulate the measured water table depths at 10 groundwater observation wells and (2) capture the tritium-based bedrock groundwater age estimates from samples collected at the 10 groundwater observation wells, as well as tritium-based stream water transit time estimates made at two locations along the M8 stream network (sampling locations are shown in Figure 1b). The best set of calibrated parameters ($K_t$, $K_b$, and $R$) was manually obtained to achieve two best (maximum) Nash-Sutcliffe (NS) values between simulated and observed/estimated (1) water table depths and (2) groundwater (and stream) ages. We also calculated the ranges for each of the calibrated parameters in which two NS values are within 10% of the best NS values. A formal uncertainty analysis is beyond the scope of this study, but the mentioned analysis provides some general insights into the uniqueness of the calibrated parameters and the sensitivity of modeled results to the calibrated parameters. Finally, the calibrated model was validated for its ability to match the base flow values calculated from long-term flow observations at the M8 catchment (165 mm/year; median long-term base flow) and at the Powerline Creek outlet (624 mm/year).

### 2.6. Virtual Experiments

Once our model was parameterized and assessed based on the hydrometric and tracer field data, we then used the model to perform a series of virtual experiments (Weiler & McDonnell, 2004) to explore the impacts of different controls on groundwater flow from the Maimai headwater catchments and their subsidies to their larger watershed. In this virtual experimentation approach, we explored the impact of different controls by changing the value of one (control) and keeping all else the same and without any further calibration.

While the list of possible variables (controls) to explore was long, the important controls—deemed important from literature reviews (e.g., Bresciani et al., 2016) and our own recent field work at the Maimai (Gabrielli, 2017)—we assessed, were (1) the recharge rate, (2) the regional topographic relief roughness or average watershed slope, and (3) the average watershed (aquifer) active thickness. To explore the first control, we considered four different recharge rates equal to 4, 175, 365, and 730 mm/year. These values cover the 10th percentile to 90th percentile of long-term estimated base flow rates at the M8 catchment as explained in section 2.2 (Figure S1). At the same time, this range in recharge values represents a plausible range for recharge rate in arid to humid climates (Gleeson & Manning, 2008). To explore the impacts of watershed slope, we generated three different land surface topographies with overall average slopes of 30°, 20°, and 10° through uniform scaling of the topographic surface elevation from the original LiDaR-based land surface topography of the Maimai watershed. Note that the average slope of the Maimai watershed is 38°. This range in watershed slope (10–38°) is generally representative of slopes from other forested watersheds around the world. To explore the impacts of watershed active thickness, we adjusted the location of the no-flow boundary at the bottom of the computational domain to $Z = 100$ m, $Z = -100$ m, and $Z = -200$ m from the reference no-flow boundary at $Z = 0$ m used for the original calibrated model. This treatment leads to average watershed thicknesses of approximately 200, 400, and 500 m, respectively. In each headwater catchment shown in Figure 1a and for each virtual experiment, we calculated the headwater groundwater subsidy index ($I_s$), equal to the ratio of the number of pathlines discharging out of the headwater catchment toward Powerline Creek to all pathlines that originate from the headwater catchment. Indeed, the headwater groundwater subsidy index represents the proportion of out-of-catchment groundwater contribution from the headwater catchment to the total groundwater recharged into the headwater catchment. We calculated the M8 catchment's subsidy index and the average of all catchments' subsidy indexes toward Powerline Creek.

## 3. Results

### 3.1. Model Testing Against Hydrometric and Tracer Measurements

The calibrated groundwater flow and transport model was able to simulate the observed groundwater table depths and tritium-based groundwater age (and transit time) estimates with the best (maximum) NS values of 0.34 and 0.95, respectively, in 12 measurement locations within the M8 headwater catchment (Figure 2). The model, however, overestimated groundwater table depth along the ridgeline. This can be attributed to nonuniform thickness of the computational domain that led to a larger transmissivity along the ridgeline compared to the riparian areas.

The calibrated maximum recharge rate ($R$) was 175 mm/year. The calibrated values of saturated hydraulic conductivities of the top ($K_t$) and bottom ($K_b$) bedrock layers were $1.15 \times 10^{-7}$ and $1.05 \times 10^{-8}$ m/s, respectively. The ranges for calibrated parameters in which two NS values were within 10% of the best NS values are 155–185 mm/year for recharge rate, $9.95 \times 10^{-8}$ to $1.20 \times 10^{-7}$ m/s for $K_t$, and $8.50 \times 10^{-9}$ to $6.10 \times 10^{-8}$ for $K_b$. The flow model predicted groundwater base flow rate at the M8 Weir of 168 mm/year, consistent with the median long-term base flow of 165 mm/year. The simulated groundwater base flow at the Powerline Creek was 621 mm/year consistent with the annual base flow at the Maimai watershed outlet (624 mm) estimated in the previous studies.

### 3.2. Groundwater Subsidies From the Headwater Catchments to the Larger Maimai Watershed

The simulated $M_{ed}TT$ and $M_{ed}FL$ corresponded to all pathlines between recharge zones in the M8 catchment and discharge zones (both out of and within the M8 catchment) were 111 years and 209 m, respectively. $M_{ed}TT$ corresponding to the pathlines discharged out of the M8 catchment boundary into Powerline Creek was 415 years, while $M_{ed}TT$ corresponding to the pathlines discharged within the M8 catchment boundary were significantly younger (48 years). The calibrated model also showed the M8 catchment's subsidy index

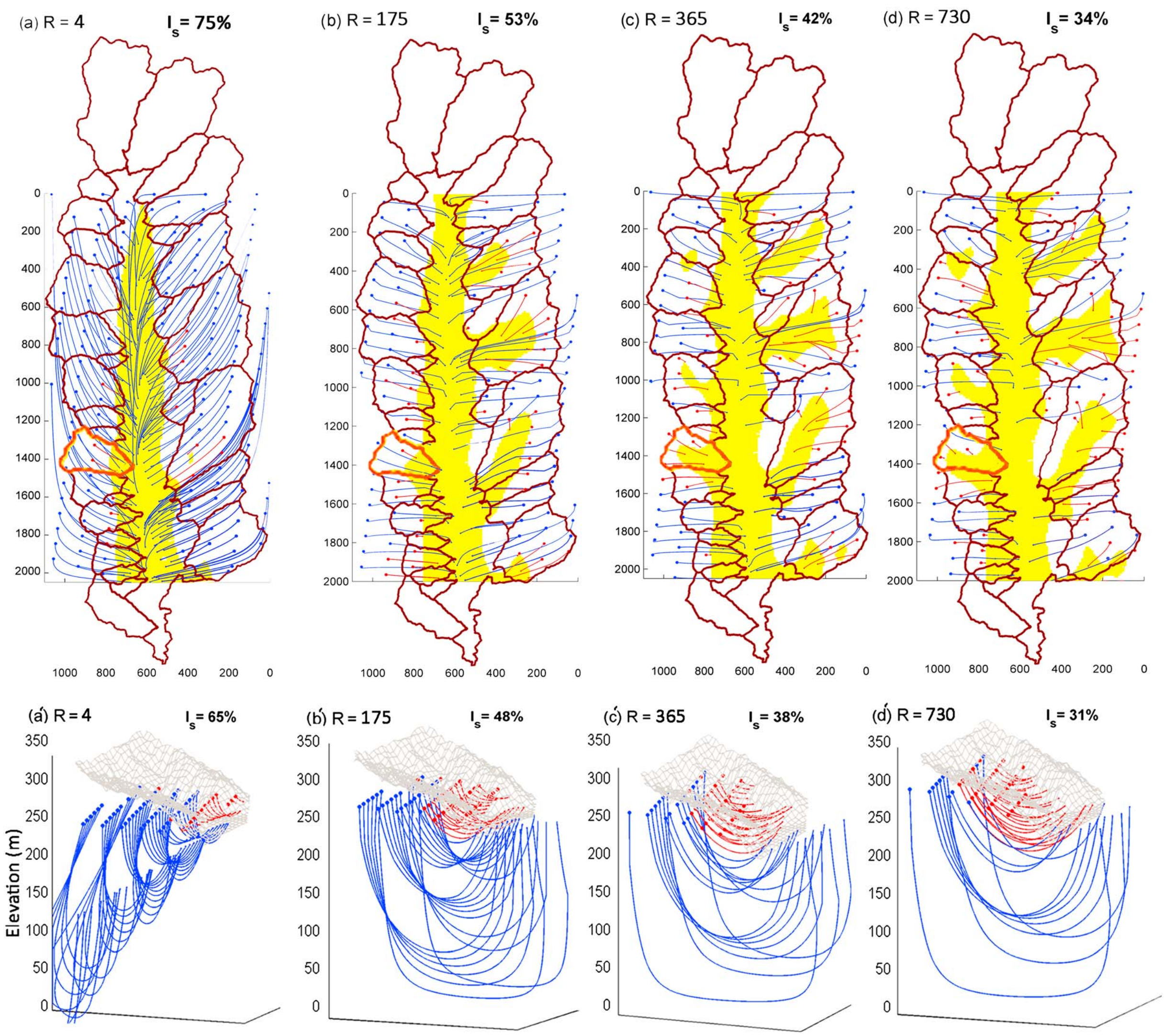

**Figure 3.** Impacts of recharge rate (*R* [mm/year]) on the distribution of groundwater flow pathlines and headwater groundwater flow subsidies at the entire Maimai watershed (a, b, c, and d) and the M8 catchment (a′, b′, c′, and d′). (a) and (a′) $R = 4$ mm/year, (b) and (b′) $R = 175$ mm/year (reference model), (c) and (c′) $R = 365$ mm/year, and (d) and (d′) $R = 730$ mm/year. Blue (and red) lines refer to pathlines discharged out of (and within) the headwater catchments. $I_s$ is the subsidy index referring to the proportion of out-of-catchment groundwater contribution to total groundwater recharged into the headwater catchment. $I_s$ in the upper panel is the average subsidy index for all headwater catchments and in the lower panel is the subsidy index for the M8 catchment. The yellow map shows the simulated locations of groundwater discharge areas. Only 1/20 of all generated pathlines are shown in the upper panel due to visualization restrictions.

($I_s$) of 48% (Figure 3b′). Indeed, 48% of recharge water into M8 catchment discharged out of the catchment boundary into Powerline Creek.

The calibrated model was then used to calculate transport features along the entire Maimai watershed. $M_{ed}$TT and $M_{ed}$FL corresponding to all pathlines between recharge and discharge zones in the entire Maimai watershed were equal to 197 years and 238 m, respectively (gray line in Figure 4). $M_{ed}$TT corresponding to the pathlines discharged out of the boundary of headwater catchments into Powerline Creek was 501 years, while $M_{ed}$TT corresponding to the pathlines discharged within the headwater catchments was 64 years. The average of all headwater catchments subsidy index ($I_s$) was 53% (Figure 3b).

With the calibrated model able to capture the hydrometric and tracer based field observations, we explored changes in the groundwater flow patterns as a result of changes in recharge rate, watershed slope, and watershed active thickness in the following sections.

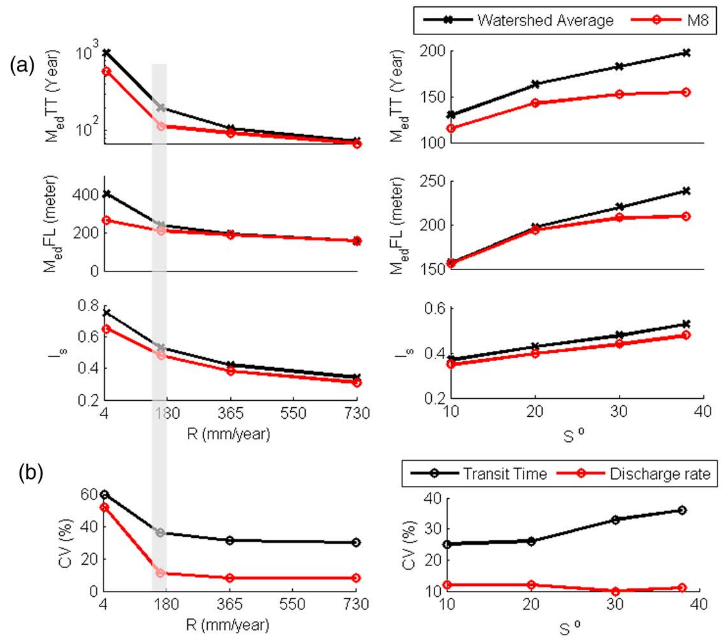

**Figure 4.** (a) Impact of recharge rate (first column), average watershed slope (second column), and watershed active thickness (third column) on $M_{ed}$TT, $M_{ed}$FL, and headwater groundwater subsidy index ($I_s$) for all headwater catchments within the Maimai watershed (black line) and the M8 headwater catchment (red line). Note that $M_{ed}$TT and $M_{ed}$FL refer to median transit time and median transit length, respectively, corresponding to all pathlines between recharge zones in parent headwater catchment and discharge zones (both out of and within the parent headwater catchment). (b) Coefficient of variation (CV) of groundwater transit times (black) and discharge rates (red) along the Maimai watershed main valley drainage system (Powerline Creek). CVs are calculated based on simulated transit times and discharge rates at 100 points located longitudinally along the length of Powerline Creek. Gray line refers to flow and transport characteristics of the M8 and the entire Maimai for the reference model.

### 3.3. Impact of Recharge Rate on Headwaters Groundwater Subsidies

As recharge rate increased, the water table elevation rose, and a larger number of low-order stream valleys throughout the entire watershed became groundwater seepage faces (yellow surface in Figure 3). This led to a higher proportion of short groundwater flow pathlines (red lines in Figure 3) that discharged into the low-order stream valleys within headwater catchments and resulted in a lower $M_{ed}$TT and $M_{ed}$FL between recharge zones and discharge zones (Figure 4a, column 1). The M8 subsidy index and the average subsidy index for all headwater catchments feeding Powerline Creek also decreased (Figure 4a, column 1).

An increase in the rate of recharge lowered the proportion of cross-catchment pathlines. Long regional pathlines originating from the upslope portion of the watershed (top left and right corners of the watershed in Figure 3) that discharged into Powerline Creek shifted to medium length regional groundwater pathlines that discharged perpendicular to Powerline Creek. These changes in pathline architecture caused a more uniform groundwater discharge transit time (and length) pattern and subsidy index along the watershed. $M_{ed}$TT, $M_{ed}$FL, and $I_s$ for M8 became more similar to the average of all headwater catchments along the watershed (Figure 4a, column 1). A recharge rate increase also increased the percentage of discharge area ($A_d$) and created a more uniform groundwater discharge rate along seepage faces throughout the entire watershed (Figure 5). In addition, the coefficient of variation of transit times and groundwater discharge rates along (the length of) Powerline Creek decreased (Figure 4b, column 1). In general, with increased recharge rate, both the flow and transport characteristics became more uniform throughout the watershed including along the Powerline Creek, and the behavior of the M8 headwater catchment became more representative of the average behavior of the entire watershed. Finally, with an increase in recharge rate from 4 to 730 mm/year, the coefficient of variation of watershed-scale groundwater table depth decreased from 16.5% to 7.5%. This implies that the water table departs less from the land surface topographic configuration as the recharge rate increases.

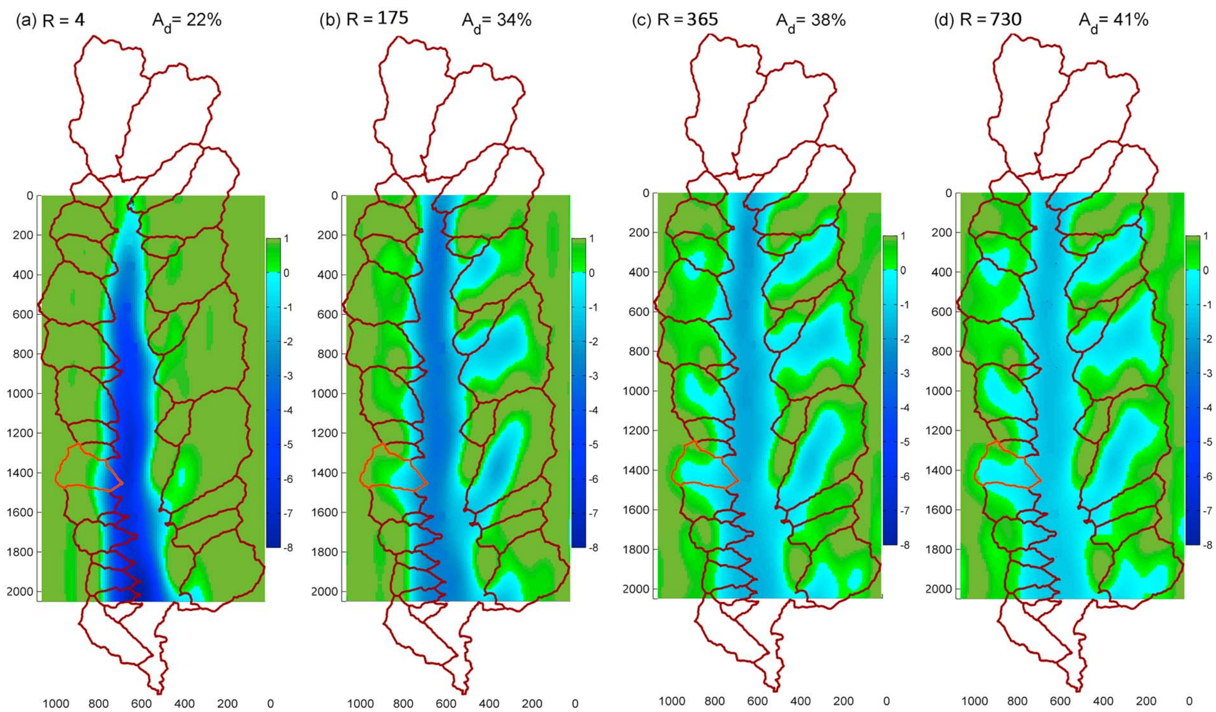


**Figure 5.** Impact of recharge rate (*R* [mm/year]) on the distribution of recharge (green) and discharge (blue) flux rates at the Maimai watershed. The color map shows the distribution of normalized discharge/recharge fluxes with respect to corresponding recharge rates. Parameter $A_d$ refers to the percentage of discharge area in the entire computational domain. (a) $R = 4$, (b) $R = 175$, (c) $R = 365$, and (d) $R = 730$.

### 3.4. Impact of Watershed Slope on Headwater Groundwater Subsidies

With hypothetical decreases in average slope of the watershed, the extension of seepage faces (yellow surface in Figure 6) increased as the water table intersected more low-order stream valleys. This also led to an increase in the number of short groundwater flow pathlines (red lines in Figure 6) that discharged into the low-order stream valleys within headwater catchments and ultimately a decrease in $M_{ed}$TT and $M_{ed}$FL between recharge zones and discharge zones (Figure 4a, column 2). The groundwater subsidies from headwater catchments to parent watershed also decreased.

A hypothetical decrease in watershed slope did create a more uniform groundwater discharge rate throughout the watershed (Figure 7), similar to the effect seen with an increase in recharge rate. Indeed, groundwater discharge rate at the low-order stream valleys became more similar to the groundwater discharge rates at the high-order stream valleys. In addition, $M_{ed}$TT, $M_{ed}$FL, and $I_s$ for M8 became more similar to the average of all headwater catchments along the watershed (Figure 4a, column 2). In general, with a hypothetical decrease in watershed slope, simulated flow and transport characteristics within M8 became more aligned with the flow and transport characteristics of the entire watershed. The slope of the land surface, however, had less impact on flow and transport characteristics compared to the recharge rate as discussed in section 3.3 for the range of variables considered in this paper. Furthermore, decreases in watershed slope from 38° to 10° significantly reduced the coefficient of variation of watershed-scale water table depth from 13.7% to 1.2%. This implies that the water table further follows the land surface topographic configuration as the landscape topography becomes gentler.

### 3.5. Impact of Watershed Active Thickness on Headwaters Groundwater Subsidies

An increase in watershed active thickness slightly increased $M_{ed}$TT, $M_{ed}$FL, and groundwater flow subsidy from headwater catchments toward Powerline Creek (Figure 4a, column 3). The extension of groundwater discharge areas slightly decreased as active aquifer thickness increased (not shown here). In addition, increases in watershed active thickness from 200 to 500 m increased only slightly (from 12.9% to 13.90%) the coefficient of variation in groundwater table depth along the watershed.

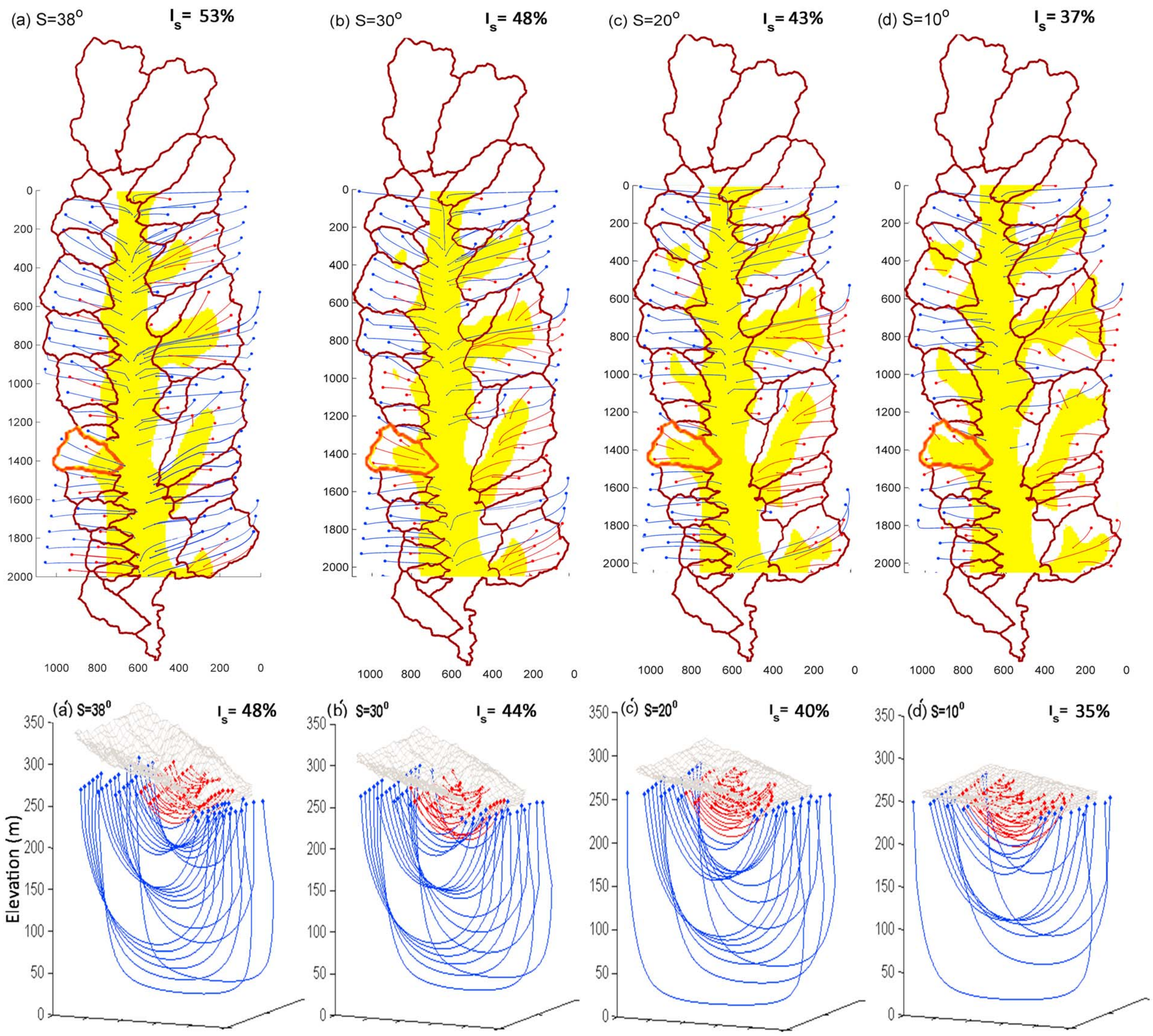


**Figure 6.** Impacts of average land surface slope (*S*) on the distribution of groundwater flow pathlines and headwater groundwater flow subsidies for the entire watershed (a, b, c, and d) and the M8 catchment (a′, b′, c′, and d′). (a) and (a′) *S* = 38° (reference model), (b) and (b′) *S* = 30°, (c) and (c′) *S* = 20°, and (d) and (d′) *S* = 10°. Blue (and red) lines refer to pathlines discharging out of (and within) the headwater catchments. Only 1/20 of all generated pathlines are shown in the upper panel due to visualization restrictions.

## 4. Discussion

Our study is one of the first that we are aware of that brings together field and modeling approaches—constrained with tracer and groundwater age, stream transit time, water table head data, and hydrogeological characterization—to determine headwaters groundwater subsidies to their parent watershed. Our modeling results showed that the new semianalytical integrated flow and transport model of Ameli and Craig (2014) was able to predict the available hydrometric and tracer field observations. Only a small range for groundwater recharge rates and saturated hydraulic conductivities of the upper part of bedrock formation were able to replicate the field observations. This suggests that a watershed tracer and hydrometric (groundwater) responses are sensitive to these well-constrained parameters.

### 4.1. Controls on Headwater Groundwater Subsidy to the Parent Watershed

Our reference model (calibrated with hydrometric and age observations from field data) showed that 48% of the groundwater recharged within the 4.5 ha M8 headwater catchment discharged out of the M8 catchment and into its larger parent watershed. These groundwater *losses* from the M8 catchment are significant,

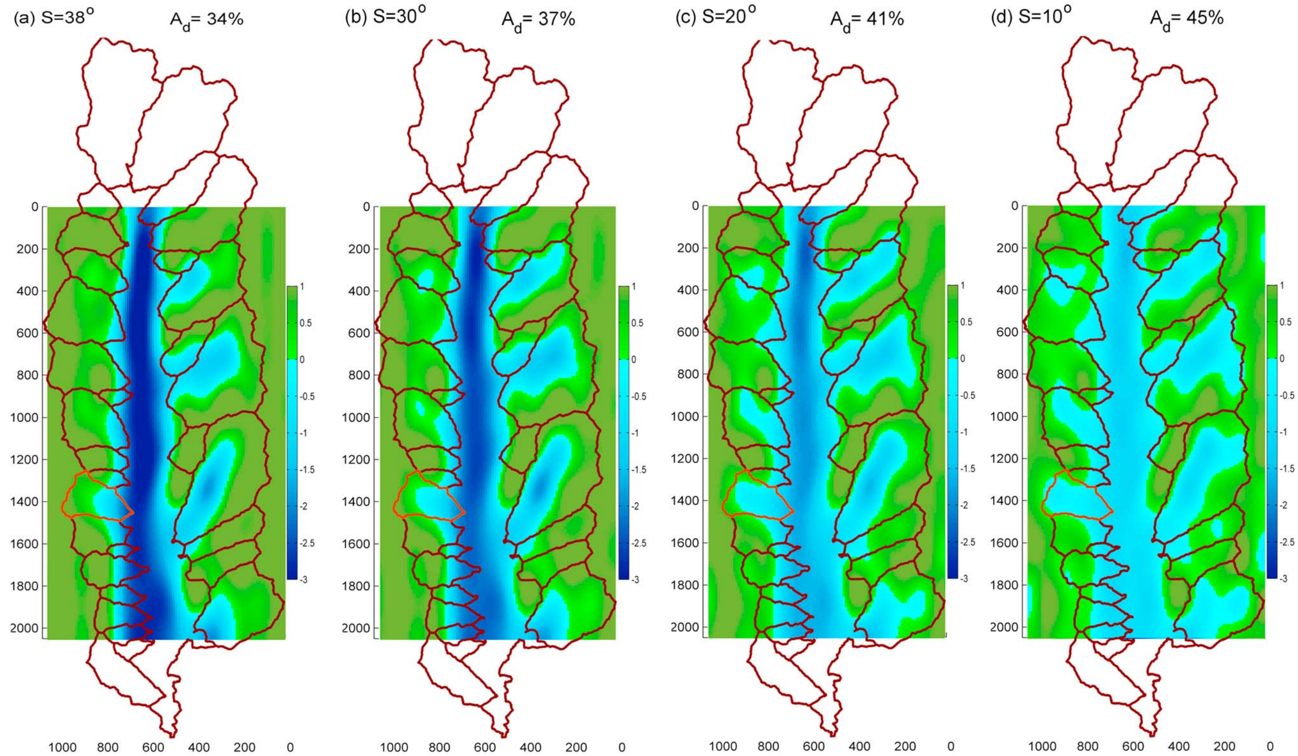


**Figure 7.** Impact of land surface slope (*S*) on the distribution of recharge (green) and discharge (blue) fluxes at the Maimai watershed. The color map shows the distribution of normalized discharge/recharge fluxes with respect to the applied recharge rate (calibrated recharge rate equal to 175 mm/year). Parameter $A_d$ refers to the percentage of discharge area in the entire watershed. (a) $S$ = 38°, (b) $S$ = 30°, (c) $S$ = 20°, and (d) $S$ = 10°.

especially for a catchment whose bedrock has been generally described as *poorly permeable* (Mosley, 1979). Also notable is the large difference between the simulated groundwater ages at depth and the previously reported young streamflow age within the M8 catchment (on the order of months; Pearce et al., 1986). This reflects a system type similar to the theory proposed by Berghuijs and Kirchner (2017) where groundwater can be much older than the streamflow when most of the streamflow originates from the highly conductive soil layer above the bedrock groundwater which produces subsurface stormflow (cf. Ameli et al., 2015). Such an interpretation is supported by the recent work of Gabrielli (2017). Our model showed that outflow from the parent watershed (at Powerline Creek) was composed of 621 mm/year of subsidized groundwater from its headwaters or 37% of the total annual streamflow (of 1,660 mm/year). This base flow groundwater contribution from headwaters has previously been shown to impact water quality (e.g., silica concentration) of the Powerline Creek outflow (McGlynn et al., 2004).

Our virtual experiment results suggest that recharge rate and average watershed slope can significantly affect the magnitude, age, and flow paths of headwaters groundwater subsidies. These factors also control groundwater table location and the spatial distribution of groundwater discharge-recharge areas. As recharge rates decrease, the areal extent of seepage faces (discharge zones) decreases which leads to a lower proportion of local flow within headwater catchments and a higher proportion of regional groundwater flow out of the headwater catchments toward the higher-order stream. In addition, high-relief watersheds generally showed a larger proportion of groundwater flow exports from headwaters to the higher-order stream compared to the low-relief systems. These findings are consistent with previous modeling studies (Gleeson & Manning, 2008; Holzbecher, 2001; Welch & Allen, 2012) and field work (Genereux et al., 2002; Winter et al., 2003) that have described a larger proportion of streamflow (or lake water) being sourced from regional groundwater compared to local groundwater in high-relief landscapes and/or dry climatic conditions.

Our reference model results also showed long transit time of 501 years for groundwater discharging from headwater catchments into the main valley drainage system of the Maimai watershed. This transit time was significantly larger than the transit time for groundwater discharging within the headwaters (64 years).

10.1029/2017WR022356

These values are somewhat consistent with other studies. For example, Kolbe et al. (2016) reported a transit time for *local and intermediate* groundwater flow of greater than 50 years into a 35 km$^2$ agricultural watershed. Goderniaux et al. (2013) suggested a mean transit time of thousands of years for deep regional groundwater flow into a large, 1,400 km$^2$ watershed. Our virtual experiment showed that as the watershed slope increased, the transit time and flow length of headwaters groundwater subsidies toward higher-order stream increased. This finding is supported by recent tracer-based global observations which have shown that steeper catchments have a higher proportion of old streamflow (Jasechko et al., 2016). Using a water balance approach, Sayama et al. (2011) also showed that steeper watersheds stored greater volumes of water, and thus, they would have longer mean transit times compared to watersheds with lower topographic gradients under similar recharge conditions.

### 4.2. Free-Surface Versus Topography-Driven Approaches to Quantify Headwater Groundwater Subsidy

The widely used topography-driven assumption (Toth, 1963), where the water table is assumed to be a replica of land surface, was not valid for most of the examples solved in this paper. The coefficient of variation of simulated watershed-scale water table depth was large for most examples (except for the lowest topographic relief roughness) implying that the water table depth largely varies along the watershed and water table configuration rarely followed the land surface configuration. Our results showed that as recharge rate decreased and/or average watershed slope increased, the spatial variation of water table depth along the watershed increased, and the water table configuration departed further from the topographic surface configuration. This leads to a larger difference between the groundwater divide and the surface water divide (obtained through topographic analysis) of high-order streams and is consistent with the numerical modeling study of Tiedeman et al. (1997) who showed that the groundwater watershed was 50% larger than the surface water watershed for a regional water body within a dry and steep landscape. Gleeson and Manning (2008) and Haitjema and Mitchell-Bruker (2005) also theoretically showed that recharge rate and watershed relief control topography-driven versus recharge-driven water tables.

Results also showed a substantial difference in the characteristics of headwater groundwater subsidy (e.g., magnitude, transit time, and transit length) between situations where water table configuration departed from the land surface topography and situations where water table (to some extent) follows the land surface topography. Thus, the treatment of groundwater table as a *free-surface* condition, where a priori unknown location of groundwater table is calculated as part of the solution, provides a more reliable estimate of sources, transit times, and flow paths of local and regional groundwater flow, critically required for an efficient future ecosystem and water quality/quantity management and policy design work. This has also been emphasized in the recent studies that suggest that the groundwater table should be viewed as a variable interface changing by groundwater systems' properties and environmental changes (Bresciani et al., 2016; Condon & Maxwell, 2015; Kolbe et al., 2016). Of course, the meshless nature of the model used in our paper can further facilitate the implementation of the free-surface condition, as mesh definition and discretization in general may cause some difficulties in the incorporation of free-surface condition (see An et al., 2010, for more details).

### 4.3. Open Questions at Maimai and Elsewhere Regarding Headwater Groundwater Subsidy

Our virtual experiments suggest that there are conditions under which the simulated flow and transport characteristics within the M8 catchment become strikingly similar to that of the average of all other catchments located in the Maimai watershed (Figure 4a). These similarities are enhanced as the recharge rate increases and/or watershed slope decreases. Of course, this finding can be the consequence of (1) an unusually homogenous geology of the underlying Old Man Gravels (as discussed by Pope et al., 2000), (2) our hypothesized uniform lateral patterns of saturated hydraulic conductivity observed in the Maimai watershed (McGlynn et al., 2004), and (3) highly organized topographic structure as discussed for this system since the early work of Mosley (1979). All of this opens new avenues for future hydrology and water quality studies in the Maimai watershed (and elsewhere) to leverage these possible scaling relations or new hydrological and biogeochemical understanding. The observed similarities between M8 catchment's response and the rest of watershed's response raise the following question: Under which structural and climatic conditions might the watershed's hydrological and biogeochemical responses become simply the linear sum of their headwater catchments' responses? Or conversely, under which condition can the study of one headwater catchment guide the understanding of the entire watershed response? These would be fruitful questions to go after, building on earlier work of Shaman et al. (2004) and Uchida et al. (2005) on the linearity of watershed response.

New field indicators may also guide the prediction of the magnitude and linearity of headwater groundwater subsidy at the Maimai watershed. Our virtual experiments suggest that as the degree of longitudinal variability in groundwater age (and groundwater discharge rate) along the Powerline Creek decreases (due to an increase in recharge rate; Figure 4b, first column), the linearity of headwaters groundwater response enhances, while the proportion of out-of-catchment groundwater subsidy decreases (Figure 4a, first column). This may raise the following question: To what extent can longitudinal measurements of flow and tracers along the high-order stream over a period of time guide the prediction of temporal changes in (1) the proportion of out-of-catchment groundwater subsidy, (2) the linearity of watershed response, and (3) recharge rate at the Maimai watershed? In many ways, this is M. G. Anderson and Burt (1978) revisited—where instead of their work documenting the discharge of subsurface stormflow from hollows to a stream reach, the question today is one of deeper connections and processes and accounting for both flow and transport.

Elsewhere, understanding of the controls on transit time, flow paths, and the magnitude of headwaters groundwater subsidies may have important implications for developing large-scale water quality management and source water protection strategies and designing future field and groundwater modeling experiments. Groundwater subsidies from headwater catchments can provide high-order stream with old waters that have high concentrations of major ions (Genereux et al., 2002) and solutes (Van Meter et al., 2018). Our results showed that the age, source, and flow paths (and therefore the concentration) of such old water changes with recharge rate, implying that a watershed's water quality response may alter under changing climate. New research is needed to explore the large simulated values of the transit time of the groundwater subsidies determined in this paper and in other similar studies. Such large transit time may suggest that the water quality response time to management practices is long and that current water quality status in the watershed can be related to past land use practices of the watershed and surrounding basins (as also suggested in Hrachowitz et al., 2016; McDonnell & Beven, 2014; Morgenstern et al., 2014). Our results suggest that this response time becomes longer and the proportion of regional groundwater subsidy becomes larger as recharge rate decreases; the decrease in recharge rate is a potential future scenario for much of the earth surface stemmed from future global warming and land development (Gleeson et al., 2016).

## 5. Conclusion

We linked a new dense groundwater well network in the well-studied Maimai watershed and a new physically based semianalytical integrated flow and transport model to quantify the groundwater flow out of headwater catchments and their subsidies to their parent watershed. The meshless nature of the model facilitated an efficient implementation of the free-surface condition for delineating the a priori unknown location of the water table, as well as an efficient characterization of local and regional groundwater flow paths and transit times. The model was able to simulate the flow and tracer observations in the M8 catchment and watershed outlet. The model showed that almost 50% of groundwater that was recharged in the M8 headwater catchment discharged outside of the headwater catchment divide and subsidized the main valley drainage network of the Maimai watershed. Along the entire watershed, 53% of groundwater recharge that occurs within the headwater catchments is subsidized to their parent watershed. Our virtual experiments showed that the relative proportion of this headwater groundwater subsidy increased as recharge rate decreased and/or watershed slope increased. The findings of this paper have implications for the management of groundwater resource quality/quantity and their interaction with the other elements of hydrologic cycle. Our findings also guide the interpretation of field indicators to predict the controls on groundwater subsidy from headwater catchments.

**Acknowledgments**
We thank John Payne at Landcare NZ for his continued commitment to the Maimai watershed. We thank Mike Stewart for useful ongoing discussions. We thank Kim Janzen for her useful feedback. J. J. M. thanks the NSERC Discovery Grant and Accelerator Grant program for funding this work. C. G. thanks AGU Horton Research Grant for funding of his studies at the Maimai watershed. The details of the methodology and its parameters, needed to evaluate the conclusions of the paper, are presented in the supporting information.

## References

Ameli, A. A., Beven, K., Erlandsson, M., Creed, I., McDonnell, J., & Bishop, K. (2017). Primary weathering rates, water transit times and concentration-discharge relations: A theoretical analysis for the critical zone. *Water Resources Research*, *52*, 942–960. https://doi.org/10.1002/2016WR019448

Ameli, A. A., Craig, J., & McDonnell, J. (2015). Are all runoff processes the same? Numerical experiments comparing a Darcy-Richards solver to an overland flow-based approach for subsurface storm runoff simulation. *Water Resources Research*, *51*, 10,008–10,028. https://doi.org/10.1002/2015WR017199

Ameli, A. A., & Craig, J. R. (2014). Semianalytical series solutions for three-dimensional groundwater-surface water interaction. *Water Resources Research*, *50*, 3893–3906. https://doi.org/10.1002/2014WR015394
Ameli, A. A., Craig, J. R., & Wong, S. (2013). Series solutions for saturated–unsaturated flow in multi-layer unconfined aquifers. *Advances in Water Resources*, *60*, 24–33. https://doi.org/10.1016/j.advwatres.2013.07.004
An, H., Ichikawa, Y., Tachikawa, Y., & Shiiba, M. (2010). Three-dimensional finite difference saturated-unsaturated flow modeling with non-orthogonal grids using a coordinate transformation method. *Water Resources Research*, *46*, W11521. https://doi.org/10.1029/2009WR009024
Anderson, M. G., & Burt, T. (1978). The role of topography in controlling throughflow generation. *Earth Surface Processes*, *3*(4), 331–344. https://doi.org/10.1002/esp.3290030402
Anderson, M. P., Woessner, W. W., & Hunt, R. J. (2015). *Applied groundwater modeling: Simulation of flow and advective transport*. Academic Press. https://doi.org/10.1016/B978-0-08-091638-5.00017-1
Bear, J. (1972). *Dynamics of fluids in porous media* (p. 764). New York: Eisevier.
Berghuijs, W. R., & Kirchner, J. W. (2017). The relationship between contrasting ages of groundwater and streamflow. *Geophysical Research Letters*, *44*, 8925–8935. https://doi.org/10.1002/2017GL074962
Bowen, F. (1967). Early Pleistocene glacial and associated deposits of the West Coast of the South Island, New Zealand. *New Zealand Journal of Geology and Geophysics*, *10*(1), 164–181. https://doi.org/10.1080/00288306.1967.10428188
Bresciani, E., Gleeson, T., Goderniaux, P., de Dreuzy, J., Werner, A., Wörman, A., et al. (2016). Groundwater flow systems theory: Research challenges beyond the specified-head top boundary condition. *Hydrogeology Journal*, *24*(5), 1087–1090. https://doi.org/10.1007/s10040-016-1397-8
Cardenas, M. B., & Jiang, X.-W. (2010). Groundwater flow, transport, and residence times through topography-driven basins with exponentially decreasing permeability and porosity. *Water Resources Research*, *46*, W11538. https://doi.org/10.1029/2010WR009370
Carey, S. K., Tetzlaff, D., Seibert, J., Soulsby, C., Buttle, J., Laudon, H., et al. (2010). Inter-comparison of hydro-climatic regimes across northern catchments: Synchronicity, resistance and resilience. *Hydrological Processes*, *24*(24), 3591–3602. https://doi.org/10.1002/hyp.7880
Cartwright, I., Irvine, D., Burton, C., & Morgenstern, U. (2018). Assessing the controls and uncertainties on mean transit times in contrasting headwater catchments. *Journal of Hydrology*, *557*, 16–29. https://doi.org/10.1016/j.jhydrol.2017.12.007
Condon, L. E., & Maxwell, R. M. (2015). Evaluating the relationship between topography and groundwater using outputs from a continental-scale integrated hydrology model. *Water Resources Research*, *51*, 6602–6621. https://doi.org/10.1002/2014WR016774
Fiori, A., & Russo, D. (2008). Travel time distribution in a hillslope: Insight from numerical simulations. *Water Resources Research*, *44*, W12426. https://doi.org/10.1029/2008WR007135
Freeze, R. A., & Witherspoon, P. (1967). Theoretical analysis of regional groundwater flow: 2. Effect of water-table configuration and subsurface permeability variation. *Water Resources Research*, *3*(2), 623–634. https://doi.org/10.1029/WR003i002p00623
Gabrielli, C. P. (2017). *Groundwater in headwater catchments: Processes, patterns, storage and transit time*. Saskatoon, SK: University of Saskatchewan.
Gardner, W. P., Harrington, G. A., Solomon, D. K., & Cook, P. G. (2011). Using terrigenic 4He to identify and quantify regional groundwater discharge to streams. *Water Resources Research*, *47*, W06523. https://doi.org/10.1029/2010WR010276
Genereux, D. P., Wood, S. J., & Pringle, C. M. (2002). Chemical tracing of interbasin groundwater transfer in the lowland rainforest of Costa Rica. *Journal of Hydrology*, *258*(1–4), 163–178. https://doi.org/10.1016/S0022-1694(01)00568-6
Gleeson, T., Befus, K. M., Jasechko, S., Luijendijk, E., & Cardenas, M. B. (2016). The global volume and distribution of modern groundwater. *Nature Geoscience*, *9*(2), 161–167. https://doi.org/10.1038/ngeo2590
Gleeson, T., & Manning, A. H. (2008). Regional groundwater flow in mountainous terrain: Three-dimensional simulations of topographic and hydrogeologic controls. *Water Resources Research*, *44*, W10403. https://doi.org/10.1029/2008WR006848
Goderniaux, P., Davy, P., Bresciani, E., Dreuzy, J. R., & Borgne, T. (2013). Partitioning a regional groundwater flow system into shallow local and deep regional flow compartments. *Water Resources Research*, *49*, 2274–2286. https://doi.org/10.1002/wrcr.20186
Golden, H., Creed, I. F., Ali, G., Basu, N. B., Neff, B. P., Rains, M. C., et al. (2017). Integrating geographically isolated wetlands into land management decisions. *Frontiers in Ecology and the Environment*, *15*(6), 319–327. https://doi.org/10.1002/fee.1504
Haitjema, H. M., & Mitchell-Bruker, S. (2005). Are water tables a subdued replica of the topography? *Ground Water*, *43*(6), 050824075421008.
Harrington, G. A., Gardner, W. P., & Munday, T. J. (2014). Tracking groundwater discharge to a large river using tracers and geophysics. *Groundwater*, *52*(6), 837–852. https://doi.org/10.1111/gwat.12124
Hayashi, M., & Rosenberry, D. O. (2002). Effects of ground water exchange on the hydrology and ecology of surface water. *Ground Water*, *40*(3), 309–316. https://doi.org/10.1111/j.1745-6584.2002.tb02659.x
Holzbecher, E. (2001). The dynamics of subsurface water divides—Watersheds of Lake Stechlin and neighbouring lakes. *Hydrological Processes*, *15*(12), 2297–2304. https://doi.org/10.1002/hyp.261
Hrachowitz, M., Benettin, P., Breukelen, B. M., Fovet, O., Howden, N. J., Ruiz, L., et al. (2016). Transit times—The link between hydrology and water quality at the catchment scale. *Wiley Interdisciplinary Reviews: Water*, *3*(5).
Hwang, T., Band, L. E., Vose, J. M., & Tague, C. (2012). Ecosystem processes at the watershed scale: Hydrologic vegetation gradient as an indicator for lateral hydrologic connectivity of headwater catchments. *Water Resources Research*, *48*, W06514. https://doi.org/10.1029/2011WR011301
Janković, I., Fiori, A., & Dagan, G. (2003). Flow and transport in highly heterogeneous formations: 3. Numerical simulations and comparison with theoretical results. *Water Resources Research*, *39*(9), 1270. https://doi.org/10.1029/2002WR001721
Jasechko, S., Kirchner, J. W., Welker, J. M., & McDonnell, J. J. (2016). Substantial proportion of global streamflow less than three months old. *Nature Geoscience*, *9*(2), 126–129. https://doi.org/10.1038/ngeo2636
Kolbe, T., Marçais, J., Thomas, Z., Abbott, B. W., de Dreuzy, J.-R., Rousseau-Gueutin, P., et al. (2016). Coupling 3D groundwater modeling with CFC-based age dating to classify local groundwater circulation in an unconfined crystalline aquifer. *Journal of Hydrology*, *543*, 31–46. https://doi.org/10.1016/j.jhydrol.2016.05.020
Lim, K. J., Engel, B. A., Tang, Z., Choi, J., Kim, K. S., Muthukrishnan, S., & Tripathy, D. (2005). Automated web GIS based hydrograph analysis tool, WHAT. *JAWRA Journal of the American Water Resources Association*, *41*(6), 1407–1416. https://doi.org/10.1111/j.1752-1688.2005.tb03808.x
Małoszewski, P., & Zuber, A. (1982). Determining the turnover time of groundwater systems with the aid of environmental tracers: 1. Models and their applicability. *Journal of Hydrology*, *57*(3–4), 207–231.
Manning, A. H., & Solomon, D. K. (2005). An integrated environmental tracer approach to characterizing groundwater circulation in a mountain block. *Water Resources Research*, *41*, W12412. https://doi.org/10.1029/2005WR004178
Marklund, L., & Wörman, A. (2011). The use of spectral analysis-based exact solutions to characterize topography-controlled groundwater flow. *Hydrogeology Journal*, *19*(8), 1531–1543. https://doi.org/10.1007/s10040-011-0768-4

Maxwell, R. M., & Condon, L. E. (2016). Connections between groundwater flow and transpiration partitioning. *Science*, *353*(6297), 377–380. https://doi.org/10.1126/science.aaf7891

Maxwell, R. M., Condon, L. E., Kollet, S. J., Maher, K., Haggerty, R., & Forrester, M. M. (2015). The imprint of climate and geology on the residence times of groundwater. *Geophysical Research Letters*, *43*, 701–708. https://doi.org/10.1002/2015GL066916

McCallum, J. L., Cook, P. G., & Simmons, C. T. (2015). Limitations of the use of environmental tracers to infer groundwater age. *Groundwater*, *53*(S1), 56–70. https://doi.org/10.1111/gwat.12237

McDonnell, J. J. (1990). A rationale for old water discharge through macropores in a steep, humid catchment. *Water Resources Research*, *26*(11), 2821–2832. https://doi.org/10.1029/WR026i011p02821

McDonnell, J. J., & Beven, K. (2014). Debates—The future of hydrological sciences: A (common) path forward? A call to action aimed at understanding velocities, celerities and residence time distributions of the headwater hydrograph. *Water Resources Research*, *50*, 5342–5350. https://doi.org/10.1002/2013WR015141

McDonnell, J. J., McGuire, K., Aggarwal, P., Beven, K. J., Biondi, D., Destouni, G., et al. (2010). How old is streamwater? Open questions in catchment transit time conceptualization, modelling and analysis. *Hydrological Processes*, *24*(12), 1745–1754. https://doi.org/10.1002/hyp.7796

McGlynn, B. L., McDonnel, J. J., & Brammer, D. D. (2002). A review of the evolving perceptual model of hillslope flowpaths at the Maimai catchments, New Zealand. *Journal of Hydrology*, *257*(1), 1–26.

McGlynn, B. L., McDonnell, J. J., Seibert, J., & Kendall, C. (2004). Scale effects on headwater catchment runoff timing, flow sources, and groundwater-streamflow relations. *Water Resources Research*, *40*, W07504. https://doi.org/10.1029/2003WR002494

McGuire, K. J., & McDonnell, J. J. (2006). A review and evaluation of catchment transit time modeling. *Journal of Hydrology*, *330*(3–4), 543–563. https://doi.org/10.1016/j.jhydrol.2006.04.020

Morgenstern, U., Daughney, C., Leonard, G., Gordon, D., Donath, F., & Reeves, R. (2014). Using groundwater age to understand sources and dynamics of nutrient contamination through the catchment into Lake Rotorua, New Zealand. *Hydrology and Earth System Sciences Discussions*, *11*(8), 9907–9960. https://doi.org/10.5194/hessd-11-9907-2014

Morgenstern, U., & Daughney, C. J. (2012). Groundwater age for identification of baseline groundwater quality and impacts of land-use intensification—The National Groundwater Monitoring Programme of New Zealand. *Journal of Hydrology*, *456*, 79–93.

Morgenstern, U., & Taylor, C. B. (2009). Ultra low-level tritium measurement using electrolytic enrichment and LSC. *Isotopes in Environmental and Health Studies*, *45*(2), 96–117. https://doi.org/10.1080/10256010902931194

Mosley, M. P. (1979). Streamflow generation in a forested watershed. *Water Resources Research*, *15*(4), 795–806. https://doi.org/10.1029/WR015i004p00795

Neary, D., Pearce, A., O'loughlin, C., & Rowe, L. (1978). Management impacts on nutrient fluxes in beech-podocarp-hardwood forests. *New Zealand Journal of Ecology*, 19–26.

Pearce, A. J., Stewart, M. K., & Sklash, M. G. (1986). Storm runoff generation in humid headwater catchments: 1. Where does the water come from? *Water Resources Research*, *22*(8), 1263–1272. https://doi.org/10.1029/WR022i008p01263

Person, M., Raffensperger, J. P., Ge, S., & Garven, G. (1996). Basin-scale hydrogeologic modeling. *Reviews of Geophysics*, *34*(1), 61–87. https://doi.org/10.1029/95RG03286

Pinay, G., Peiffer, S., De Dreuzy, J.-R., Krause, S., Hannah, D. M., Fleckenstein, J. H., et al. (2015). Upscaling nitrogen removal capacity from local hotspots to low stream orders' drainage basins. *Ecosystems*, 1–20.

Pope, S. E., Fahrig, L., & Merriam, H. G. (2000). Landscape complementation and metapopulation effects on leopard frog populations. *Ecology*, *81*(9), 2498–2508. https://doi.org/10.1890/0012-9658(2000)081[2498:LCAMEO]2.0.CO;2

Sayama, T., McDonnell, J. J., Dhakal, A., & Sullivan, K. (2011). How much water can a watershed store? *Hydrological Processes*, *25*(25), 3899–3908. https://doi.org/10.1002/hyp.8288

Shaman, J., Stieglitz, M., & Burns, D. (2004). Are big basins just the sum of small catchments? *Hydrological Processes*, *18*(16), 3195–3206. https://doi.org/10.1002/hyp.5739

Smerdon, B. D., Gardner, W. P., Harrington, G. A., & Tickell, S. J. (2012). Identifying the contribution of regional groundwater to the baseflow of a tropical river (Daly River, Australia). *Journal of Hydrology*, *464*, 107–115.

Thomas, Z., Abbott, B. W., Troccaz, O., Baudry, J., & Pinay, G. (2016). Proximate and ultimate controls on carbon and nutrient dynamics of small agricultural catchments. *Biogeosciences*, *13*(6), 1863–1875. https://doi.org/10.5194/bg-13-1863-2016

Tiedeman, C. R., Goode, D. J., & Hsieh, P. A. (1997). *Numerical simulation of ground-water flow through glacial deposits and crystalline bedrock in the Mirror Lake area, Grafton County*. New Hampshire: US Government Printing Office.

Toth, J. (1963). A theoretical analysis of groundwater flow in small drainage basins. *Journal of Geophysical Research*, *68*(16), 4795–4812. https://doi.org/10.1029/JZ068i016p04795

Uchida, T., Asano, Y., Onda, Y., & Miyata, S. (2005). Are headwaters just the sum of hillslopes? *Hydrological Processes*, *19*(16), 3251–3261. https://doi.org/10.1002/hyp.6004

Van Meter, K., Van Cappellen, P., & Basu, N. (2018). Legacy nitrogen may prevent achievement of water quality goals in the Gulf of Mexico. *Science*, eaar4462.

Weiler, M., & McDonnell, J. (2004). Virtual experiments: A new approach for improving process conceptualization in hillslope hydrology. *Journal of Hydrology*, *285*(1–4), 3–18. https://doi.org/10.1016/S0022-1694(03)00271-3

Weiler, M., McGlynn, B. L., McGuire, K. J., & McDonnell, J. J. (2003). How does rainfall become runoff? A combined tracer and runoff transfer function approach. *Water Resources Research*, *39*(11), 1315. https://doi.org/10.1029/2003WR002331

Welch, L., & Allen, D. (2012). Consistency of groundwater flow patterns in mountainous topography: Implications for valley bottom water replenishment and for defining groundwater flow boundaries. *Water Resources Research*, *48*, W05526. https://doi.org/10.1029/2011WR010901

Weyer, C., Peiffer, S., Schulze, K., Borken, W., & Lischeid, G. (2014). Catchments as heterogeneous and multi-species reactors: An integral approach for identifying biogeochemical hot-spots at the catchment scale. *Journal of Hydrology*, *519*, 1560–1571. https://doi.org/10.1016/j.jhydrol.2014.09.005

Wilson, J. L., & Guan, H. (2004). Mountain-block hydrology and mountain-front recharge. In F. M. Phillips, J. Hogan, & Bridget Scanlon (Eds.), *Groundwater Recharge in a Desert Environment: The Southwestern United States* (pp. 113–137). Washington, DC: American Geophysical Union.

Winter, T. C., Rosenberry, D. O., & LaBaugh, J. W. (2003). Where does the ground water in small watersheds come from? *Ground Water*, *41*(7), 989–1000. https://doi.org/10.1111/j.1745-6584.2003.tb02440.x

Zech, A., Zehner, B., Kolditz, O., & Attinger, S. (2016). Impact of heterogeneous permeability distribution on the groundwater flow systems of a small sedimentary basin. *Journal of Hydrology*, *532*, 90–101. https://doi.org/10.1016/j.jhydrol.2015.11.030